Neural Dynamics Underlying Event-Related Potentials

Ankoor S. Shah[1,2], Steven L. Bressler[3], Kevin H. Knuth[4], Mingzhou Ding[3],

Ashesh D. Mehta[5], Istvan Ulbert[6], Charles E. Schroeder[1,2*]

[1] *Department of Neuroscience, Albert Einstein College of Medicine, Bronx, NY 10461*

[2] *Cognitive Neuroscience and Schizophrenia Program, Nathan Kline Institute, Orangeburg, NY 10962*

[3] *Center for Complex Systems and Brain Sciences, Florida Atlantic University, Boca Raton, FL 33431*

[4] *Computational Sciences Division, Code IC, NASA Ames Research Center, Moffett Field, CA 94035-1000*

[5] *Department of Neurological Surgery, Weill Medical College of Cornell University, New York, NY 10021*

[6] *Institute for Psychology, Hungarian Academy of Sciences, Budapest, H-1394*

* Corresponding Author

Phone: +1-845-398-6539

Fax: +1-845-398-6545

Email: schrod@nki.rfmh.org

ABSTRACT

There are two opposing hypotheses about the brain mechanisms underlying sensory event-related potentials (ERPs). One holds that sensory ERPs are generated by phase resetting of ongoing electroencephalographic (EEG) activity, and the other that they result from signal averaging of stimulus-evoked neural responses. We tested several contrasting predictions of these hypotheses by direct intracortical analysis of neural activity in monkeys. Our findings clearly demonstrate evoked response contributions to the sensory ERP in the monkey, and they suggest the likelihood that a mixed (Evoked/Phase Resetting) model may account for the generation of scalp ERPs in humans.

TEXT

Averaged event-related potentials (ERPs) recorded from the scalp are widely used measures of the human brain's sensory and cognitive processes. There are two hypotheses about the neural origins of sensory ERPs. The more traditional view is that the stimulus "evokes" a time-locked, neural population response in each trial, and this evoked response is enhanced and clarified by signal averaging to produce the ERP (*1-4*). The alternative view is that the stimulus induces "phase resetting" of ongoing EEG rhythms in each trial, and that averaging of these phase-coherent rhythms produces the ERP (*5*).

In a recent paper, Makeig and colleagues (*6*) argued strongly against the Evoked Model in favor of the Phase Resetting Model based on scalp EEG analysis in human subjects. However, the issue is not settled, and merits further examination in light of the ambiguity of the evidence for Phase Resetting (*7*), and the strength of contrary evidence that was not considered (*11*), especially that from experiments in nonhuman primates (*13*). Moreover, earlier studies (*5, 6*) have been limited by the fact that scalp ERPs are recorded at a distance from their neural sources and by the fact that the predictions of each model were not clearly delineated. In this study, we address both limitations, first detailing the main predictions and assumptions of each model (Table 1) and then subjecting several critical requirements to direct evaluation by analyzing single-trial intracortical activity in awake, behaving monkeys.

Strict interpretations of the Phase Resetting and Evoked Models pose differing requirements for single-trial neural responses. ***(Requirement 1)*** Under Phase Resetting, activity at the dominant frequency (*19*) of the ERP must be appreciably present in the pre-stimulus period (*6*); the Evoked Model does not share this requirement. (***Requirement 2***) Under Phase Resetting, the transition from the pre- to the post-stimulus periods must involve phase concentration (i.e.,

synchronization of an EEG rhythm across trials) without a concomitant increase in power at the dominant frequency of the ERP; the Evoked Model can tolerate phase concentration but requires a post-stimulus increase in signal power.

We analyzed electrophysiological responses within areas at both low and high levels of the visual hierarchy, namely areas V1 and inferotemporal (IT) cortex, because there is evidence that the scalp ERP reflects the combined contributions from structures throughout the visual pathways (*16*). Also, we were interested in the possibility that each model describes part of the phenomenon; the Evoked Model may account better for ERP generation in cortical areas closer to the receptor surface (retina), while the Phase Resetting Model may better describe ERP contributions from areas more removed from the retina and increasingly influenced by "state" variables such as attention (*9, 20, 21*). Analysis was based on cortical electrophysiological activity sampled from two male macaque monkeys while they performed in a selective attention paradigm (*22*). The analysis focused on the neural responses to the standard, non-target stimulus in the attended condition. Neural activity profiles were sampled using linear-array multielectrodes with fourteen equally spaced contacts (either 150 or 200 μm intercontact spacing) spanning 2-2.5 mm distance (*23*). In each experimental session, a multielectrode was inserted acutely into V1 and/or IT so that the array of contacts spanned all laminae of the structure at an angle perpendicular to the lamination pattern (Figure 1A) (*24*). One-dimensional current source density (CSD) analysis was used to define the transmembrane current flow patterns generating the local field potential in the extracellular medium (*2, 25*). In each animal, two V1 and two IT recordings were analyzed for a total of four V1 and four IT experiments (*26*).

Requirement 1. The Phase Resetting Model requires that activity at the dominant frequency of the ERP be significantly present in the pre-stimulus period. Figure 1B illustrates the free-running EEG recorded from V1 of one subject during presentation of a visual stimulus at a

rate of 2/sec. A concurrent recording from an EEG electrode over the occipital brain surface near the recording site is shown (top trace) along with the recordings from all fourteen channels of the multielectrode array. This is a case with a particularly prominent evoked response, observed as a negative potential above Layer 4, which inverts to a positive potential below Layer 4 (arrows in Figure 1B) indicating that it is locally generated. The pre-stimulus activity is relatively small and displays no apparent oscillations at the frequency of the evoked response. Figure 1C uses color plots to depict the concomitant ERP (field potential), action potential (multiunit activity), and CSD across all trials in this experimental session for an electrode channel located in Lamina 4C. Again, very little pre-stimulus activity is observed across trials, and the post-stimulus period shows a discrete field potential negativity accompanied by an action potential burst and a current sink, indicating net local excitation. On the face of it, these data seem to favor the Evoked over the Phase Resetting Model. As we detail below, quantification of pre- and post-stimulus spectral features reveals that the amount of pre-stimulus oscillatory activity varies across sites in V1 (see Figure 3B), and there is more prominent baseline oscillatory activity in IT than in V1. Even in the extreme case presented in Figure 1, there is some pre-stimulus activity at the dominant frequency (Figure 1D), as required by Phase Resetting. Thus along the lines of requirement 1, we find some degree of support for each model.

Requirement 2. Phase Resetting predicts equivalence of the pre- and post-stimulus power at the dominant frequency of the ERP (*27*), while the Evoked Model predicts an increase in post-stimulus power at the dominant frequency. We tested these predictions in all four V1 sessions by examining the CSD data from one channel located in the granular layer and a second channel located in the supragranular tissue (*28*). We computed the power at the dominant frequency of the event-related response (in our case, the dominant frequency of the averaged CSD in each electrode channel considered) and calculated the pre- and post-stimulus power at this frequency

(see Supplemental Table 1). In all experimental sessions, we found significant increases in median power (Wilcoxon Signed-Rank test $p < 0.01$) and increases in the power distribution variance between the pre- to the post-stimulus periods. Figure 1D illustrates the stimulus-induced amplitude modulation at the dominant frequency in the supragranular layer during one V1 experiment in subject "V." The significant increase in power we observe clearly violates the requirement of the Resetting Model, while conforming to the requirement of the Evoked Model.

In relation to the phase concentration aspect of ***Requirement 2***, we examined the pre- and post-stimulus phase distributions at the dominant frequency for each V1 experiment. A graphic example from supragranular V1 is shown in Figure 1E. Pre-stimulus activity at the dominant frequency should yield a uniform phase distribution because stimulus presentation, which defines the pre-stimulus period, occurred with a random interstimulus interval. In three out of the four V1 sessions, pre-stimulus granular and supragranular phase distributions did not differ from a uniform distribution using a Modified Kuiper V Statistic (*29*) ($p < 0.01$), while all post-stimulus distributions were statistically different from uniformity. All post-stimulus phase distributions also exhibited a decrease in circular variance (*30*) suggesting stimulus-induced phase concentration. Although this finding does satisfy a requirement of Phase Resetting, it should be noted that the majority of the effect is due to the addition of time-locked power at the dominant frequency of the ERP as outlined above, which again argues against Phase Resetting and in favor of the Evoked Model.

To test for possible errors caused by confining the analysis to the dominant frequency and to better characterize the nature of stimulus-related responses in single trials, we performed two additional analyses. For each V1 session, we examined the single-trial power spectra in every frequency bin between 0 and 1000 Hz in the granular and supragranular data. The median post-stimulus power showed a significant increase over pre-stimulus power at all frequencies

considered in all V1 sessions (Wilcoxon Signed-Rank test, $p < 0.01$ with Bonferroni correction). Power spectra from the pre- and post-stimulus periods from one V1 session are illustrated in Figure 1F. Finally, we tested the data for an increase in total power because this property clearly demarcates the two models (Table 1). As shown in Figure 2, all layers in all experiments displayed significant increase in the median total power (Wilcoxon Signed-Rank test, $p < 0.01$). Incidentally, these results also rule out the possibility of a frequency reorganization model, which would predict that the pre- and post-stimulus power spectra would differ but that the pre- and post-stimulus total power would remain constant.

We repeated these critical analyses for all four IT sessions. In reference to ***Requirement 1***, Figure 3A shows intracortical recordings from IT with a concurrent recording at the brain surface over V1. Figure 3B depicts simultaneous recordings from V1 and IT during a different experimental session (VE7). Although, in most cases, the stimulus-evoked response is obvious, there are also clear ongoing EEG oscillations prior to stimulus presentation. Interestingly, pre-stimulus oscillations are more pronounced in IT than in V1. This amplitude difference is observed by comparing simultaneously recorded activity in V1 and IT (Figure 3B). This difference was found to be significant by quantifying the distribution of normalized pre-stimulus power at the dominant frequency for all recordings. Normalization was performed as described in Figure 2. Median normalized pre-stimulus power at the dominant frequency of the supragranular ERP increased from 0.13 $(mV/mm^2)^2$ in V1 to 0.27 $(mV/mm^2)^2$ in IT. The corresponding comparison for the granular laminae showed an increase from 0.20 $(mV/mm^2)^2$ in V1 to 0.37 $(mV/mm^2)^2$ in IT. Both increases were significant (Wilcoxon Rank-Sum test, $p < 0.01$ with Bonferroni correction). The distinct presence of pre-stimulus oscillatory activity in both V1 and IT clearly satisfies Requirement 1. However, the significant increase in pre-stimulus oscillations from V1 to

IT suggests that Phase Resetting, if present, may operate differently across the levels of the hierarchy.

In reference to ***Requirement 2***, we compared pre- and post-stimulus power and phase at the dominant frequency in both granular and supragranular laminae across cases (see example in Figure 3C). In all cases, both the median power at the dominant frequency (Wilcoxon Signed-Rank test, $p < 0.01$) and the variance of the spectral power distribution increased. Figure 3D illustrates the phase distribution at the dominant frequency of the supragranular layer for IT session V71. The pre-stimulus phase distribution is not different from a uniform distribution (Modified Kuiper V Statistic, $p < 0.01$), but the post-stimulus distribution is. The same was true throughout the data set. Post-stimulus phase concentration is also indexed by a decrease in sample circular variance between the pre- and post-stimulus periods, evident in all cases.

We also characterized the stimulus-induced power increase over frequencies outside the dominant frequency of the ERP. Comparison of the IT power spectra between the pre- and post-stimulus periods over a range of 0 to 50 Hz is illustrated in Figure 3E for the supragranular layer in one IT session. All IT sessions showed a significant post-stimulus increase in median power with respect to the pre-stimulus power in both the granular and supragranular layers across frequency bands (Wilcoxon Signed-Rank test, $p < 0.01$ with Bonferroni correction). The final test that we applied to the IT data was a comparison between the total power in the pre- and post-stimulus periods. Figure 4A and B show the distribution of total signal power across trials during the pre- and post-stimulus periods, and each session displays a significant increase in post-stimulus power with respect to the pre-stimulus power (Wilcoxon Signed-Rank test, $p < 0.01$).

To understand how our findings confirm or dispute the two opposing models of scalp ERP generation, one must consider the relationship between intracortical electrophysiology and the surface ERP. A number of studies over the past decade have established homologies between

human and simian ERP components. These monkey studies have localized the cortical generators of many major ERP components and identified underlying cellular populations and processes {(*15, 16, 21*), earlier studies reviewed by (*2*)}. Of particular relevance are findings concerning the neural origins of the N1 component, which arises from the combined contributions of many extrastriate visual areas including V4, MT, intraparietal sulcal areas, and most notably, IT (*2, 14, 16, 31*). In each of these areas, N1 (N95 in monkey) has a sharp laminar voltage gradient associated with a large amplitude sink-over-source configuration of CSD components (*32*) and a large burst of action potentials. Thus, based on these prior findings, N1 reflects phasic feedforward excitation rather than arising as a cycle of an oscillatory rhythm, a point already clearly stated by Mangun (1992) (*12*). While the issue of ERP generation by Phase Resetting was not examined in the earlier studies, evoked response contributions were obvious. Though the latencies of the N1-related evoked responses slightly differ from region to region, there is sufficient synchrony among them, so that they may manifest as a large negativity in the surface ERP recorded over the extrastriate regions (*2, 14*).

The present findings do not support the hypothesis that stimulus-induced resetting of ongoing EEG rhythms is the primary mechanism of ERP generation. In particular, the increase in post-stimulus power across a broad range of frequencies including the dominant frequency of the ERP conflicts with the predictions of the Phase Resetting Model. That said, it is worth noting that alternative explanations exist for most of the observations, which some have interpreted in terms of the Phase Resetting Model. First, ERP enhancement during trials in which pre-stimulus activity in the α band is large (*6*) may result from the fact that α rhythms and evoked responses share common frequencies because they utilize similar biophysical elements; thus, α-enhancement and ERP enhancement may both be controlled by another process (*8*). Second, although it is clearly possible that "α-ringing" represents a stimulus-induced resetting of the

rhythm, it also remains likely that α-ringing is superimposed on the evoked response and that they simply share common frequencies. Third, the N1 shown in the high-α condition by Makeig *et al.* (2002) (*6*) is not typical of that seen in other laboratories, many of which work successfully to reduce "α-intrusion" and routinely produce large, reliable N1 responses without α-ringing (*34*). And finally, Bogazc *et al.* (2002) (*37*) raise the possibility that the techniques of the Makeig *et al*. (2002) (*6*) study can lead to artifactual production of Phase Resetting, through summation of background EEG with stimulus-evoked activity.

The present findings do not negate the Phase Resetting hypothesis, but they strongly support the idea that the evoked response accounts for the local, intracortical ERP. Also in support of the Evoked Model, Rols *et al.* (*38*) showed a definitive stimulus-induced increase in signal power in macaque V1 and V4, and significantly, they did so using subdural measurements, intermediate between intracortical and scalp recordings. Collectively, these findings suggest that at least some of the components of the scalp ERP arise primarily from summation of stimulus-evoked processes distributed across sensory areas. Studies investigating ERP component generators in monkeys have begun to resolve the physiological significance of components such as N1 (*2, 16*). One thing that is clear at this point is that N1-related activity in IT and other extrastriate areas occurs as a phasic pulse of activity evoked by the visual stimulus (*2, 12, 16*).

Penny *et al.* (2002) (*39*) proposed amplitude and phase modulation as possible mechanisms for generation of the ERP and they liken these processes to the Evoked and Phase Resetting Models, respectively. Our data demonstrate empirically that amplitude and phase modulation mechanisms both operate in neocortex. However, it is also obvious that phase modulation/concentration will be detected in single-trial analyses, even when a strict evoked mechanism is operating. That is, transmembrane currents triggered by stochastic firing of the inputs to local neurons and by random non-synaptic currents will generate baseline EEG. Thus,

pre-stimulus activity will contain power in the frequency bands of the ERP, and these frequency components will likely have uniform phase distributions because the generating events are random. When a stimulus is presented, the evoked response will be produced, and it will be relatively phase-locked to stimulus presentation. Phase modulation in the form of concentration will be observed simply because there is random pre-stimulus activity in frequency bands of the ERP. Penny *et al.* (*39*) rightly point out that ruling out post-stimulus power increase in the dominant frequency of the ERP is key to identifying phase resetting; however, Makeig *et al.* (*6*) did not perform this analysis.

While we do not find support for the Phase Resetting Model as the major mechanism of sensory event-related potential components, resetting may well contribute to ERP generation. Quantitatively, the power of the baseline EEG increases in the transition from V1 to IT suggesting that there may be a shift from a pure evoked mechanism of generating the ERP at low levels of sensory processing to a mixed evoked/resetting mechanism at higher processing levels. Additionally, resetting may play an important role in cortical feedback mediated ERP components, such as the "Selection Negativity" observed in the comparison between attended and non-attended, non-target stimuli in selective attention experiments (*15, 21, 40, 41*).

TABLES

Table 1: Comparison of the Phase Resetting and the Evoked models of ERP generation.

Property	Phase Resetting Model	Evoked Model
Pre-stimulus rhythmic activity	Yes	Not necessary
Pre-stimulus activity influences post-stimulus activity	Possible	Possible
Pre- to post-stimulus increase in signal power at the dominant frequency of the ERP	No	Yes
Phase distribution of the pre-stimulus activity at the dominant frequency of the ERP	Uniform	No requirement
Pre- to post-stimulus increase in phase concentration	Yes	Likely
Pre- and post-stimulus power spectra are similar	Yes	No
Pre- to post-stimulus increase in total signal power	No	Yes

FIGURES

Figure 1: Data from V1 recording session VA2. **A.** Schematic of the multielectrode positioned in striate cortex to record from all layers simultaneously. The pial surface is at the top. **B.** EEG recorded during presentation of brief light flashes at 2/sec. Recordings from an occipital surface electrode (top trace) and from all fourteen multielectrode channels are shown. The vertical marks at the bottom indicate stimulus onset. The prominent surface-negative potential reflects the local stimulus-evoked response as it undergoes polarity inversion across Layer 4 (see arrow) (*14, 16*). Note that the baseline EEG is very small relative to the evoked response. **C.** Single-trial field potential, multiunit activity, and current-source density records from an electrode channel located in the granular layer. The pre-stimulus periods have little activity, while the post-stimulus periods show discrete responses. **D.** Power distribution at the dominant frequency of the ERP in supragranular V1 demonstrates stimulus-induced amplitude modulation. The pre- and post-stimulus median power at the dominant frequency is statistically different (Wilcoxon Signed-Rank test, $p < 0.01$). **E.** Phase distribution at the dominant frequency of the ERP in supragranular V1 illustrates stimulus-induced phase modulation. The pre-stimulus distribution cannot be statistically differentiated from a uniform distribution, but the post-stimulus phases were not uniformly distributed ($p < 0.01$). A Modified Kuiper V Statistic greater than 2.00 indicates that the distribution departs from uniformity with a significance probability of 0.01 (*29*). In addition, pre- to post-stimulus phase concentration (ie. synchrony) is apparent and measured as a decrease in sample circular variance (*29*) in the post-stimulus period with respect to the pre-stimulus period. **F.** Median pre- and post-stimulus power spectra for the supragranular CSD signal display a stimulus-induced increase in power across frequencies. The post-stimulus spectrum also shows a peak at ~40 Hz that does not appear in the pre-stimulus activity. This peak may represent new frequency components being added to the post-stimulus period, a property consistent with the Evoked Model but inconsistent with the Phase Resetting Model (Table 1). Additionally, the dominant frequency during the pre-stimulus period differs from the dominant frequency of the ERP, which is incompatible with simple phase resetting.

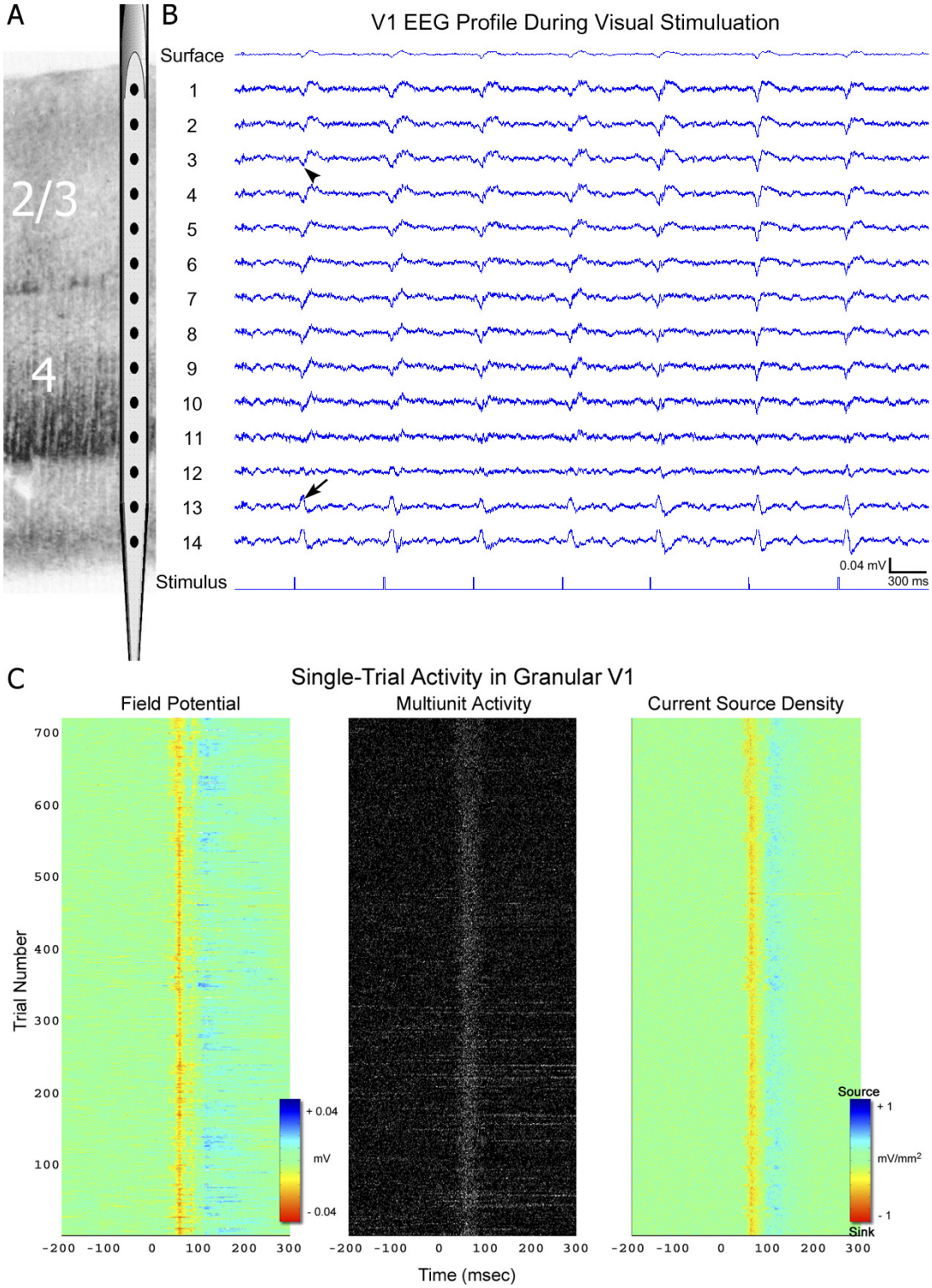
A
2/3
4
B
V1 EEG Profile During Visual Stimuluation
Surface
1
2
3
4
5
6
7
8
9
10
11
12
13
14
Stimulus
0.04 mV
300 ms
C
Single-Trial Activity in Granular V1
Field Potential
Multiunit Activity
Current Source Density
Trial Number
700
600
500
400
300
200
100
+ 0.04
mV
- 0.04
Source
+ 1
mV/mm²
- 1
Sink
-200 -100 0 100 200 300
Time (msec)

Figure 1A-C

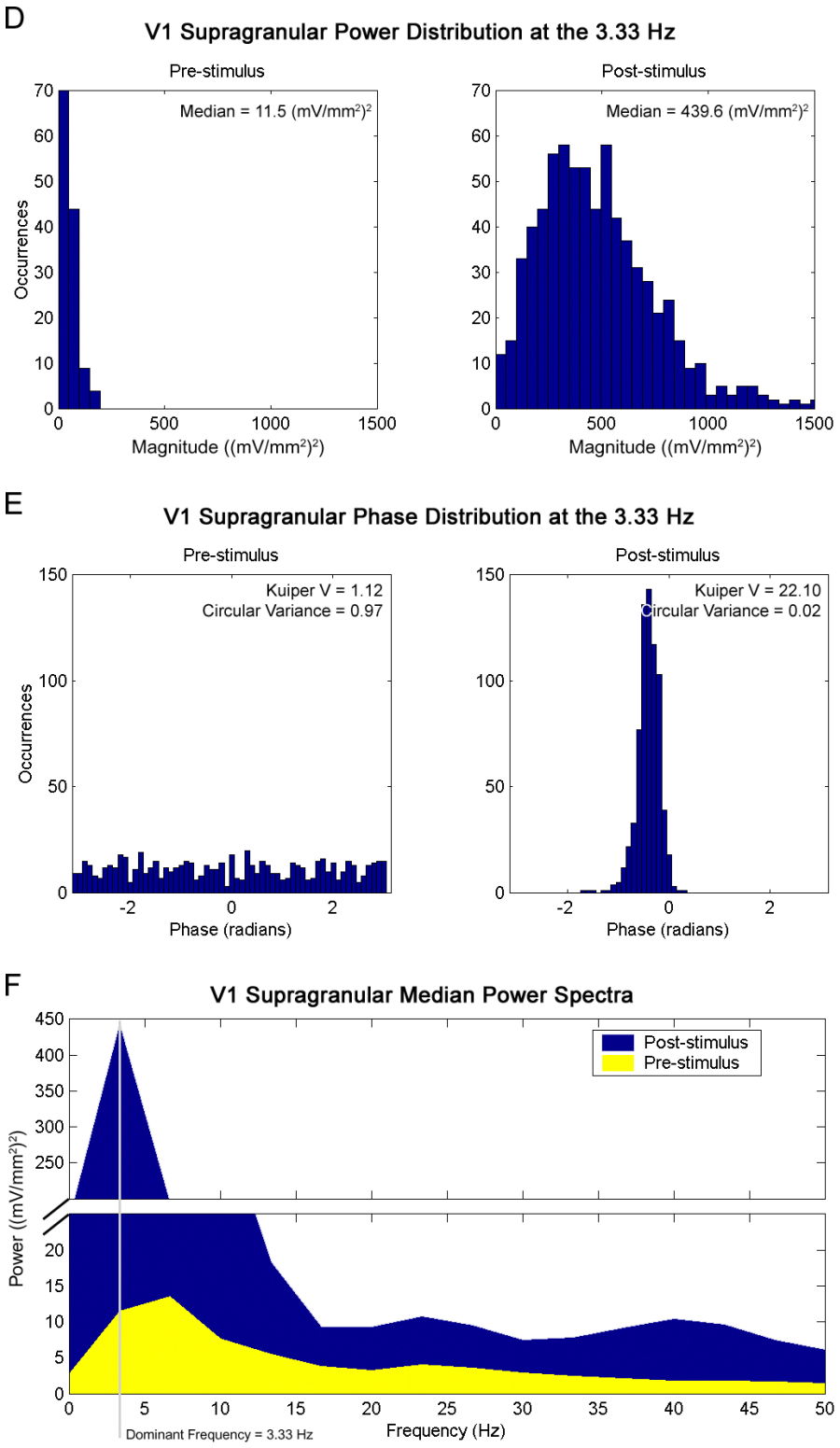
D
V1 Supragranular Power Distribution at the 3.33 Hz
Pre-stimulus
Median = 11.5 (mV/mm²)²
Post-stimulus
Median = 439.6 (mV/mm²)²
Occurrences
Magnitude ((mV/mm²)²)
E
V1 Supragranular Phase Distribution at the 3.33 Hz
Pre-stimulus
Kuiper V = 1.12
Circular Variance = 0.97
Post-stimulus
Kuiper V = 22.10
Circular Variance = 0.02
Occurrences
Phase (radians)
F
V1 Supragranular Median Power Spectra
Post-stimulus
Pre-stimulus
Power ((mV/mm²)²)
Dominant Frequency = 3.33 Hz
Frequency (Hz)

Figure 1D-F

Figure 2: Comparison of the normalized total signal power in V1 during the pre- and post-stimulus periods. Total power was calculated as the integral of the power spectrum from 0 to 1000 Hz and normalized so that the median post-stimulus total power equaled 1.0 $(mV/mm^2)^2$. The distributions of normalized power in the granular (**A**) and supragranular (**B**) layers for each V1 session are displayed graphically as box plots. The lower and upper lines of the "box" bound the 25th and 75th percentiles of the distribution, and the middle line represents that median of the sample. The position of the median line with respect to the upper and lower lines indicates the skew of the distribution. Notches in the box around the median indicate the confidence interval about that median. The lines above and below the box show the extent of the data minus outliers.

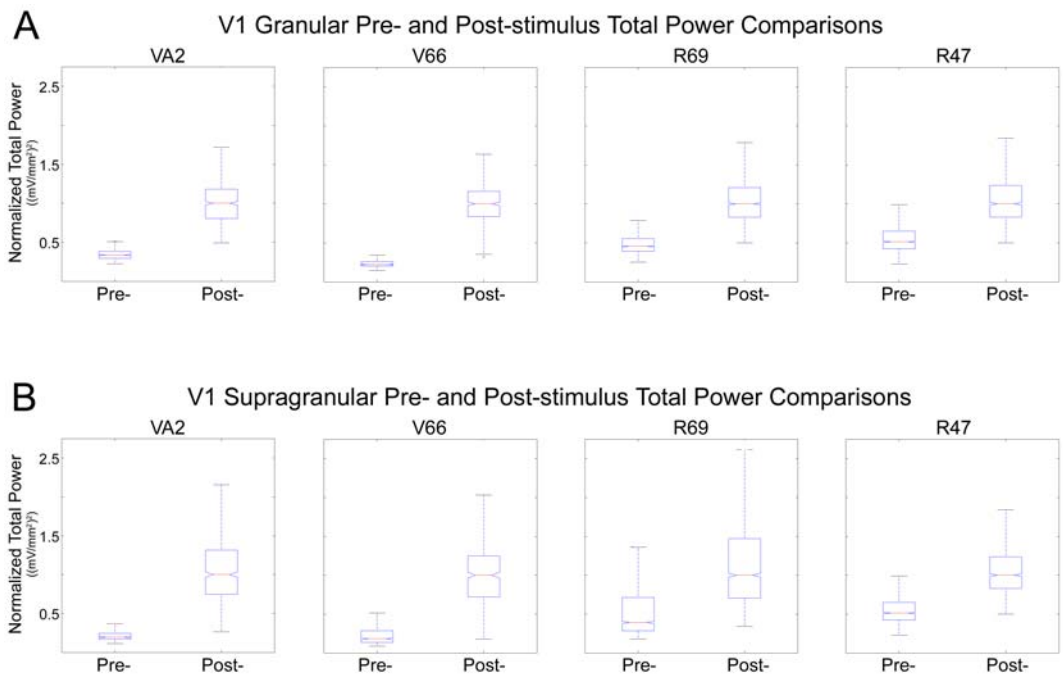

Figure 2

Figure 3: Data recorded from posterior IT of subject "V." **A.** EEG from session V71. The signal at the surface occipital electrode is also shown, and the vertical tick at the bottom of the plot denotes stimulus presentation. A clear N1 (arrow) is generated after each presentation of the stimulus. Note that Supragranular and granular responses in IT appear delayed with respect to the initial negativity (N40) recorded at the surface occipital electrode, which is largely generated in V1 {reviewed by (*2*)}. The pre-stimulus EEG activity appears to be slightly greater than that observed in V1 (see Figure 1B), but it is still notably less than the activity recorded in the post-stimulus period. **B.** EEG from session VE7. Multielectrode arrays were inserted into both V1 and IT. Pre-stimulus activity during this session displays ongoing rhythms in both areas; despite the presence of pre-stimulus rhythms, the total power in IT still demonstrates a pre- to post-stimulus increase (see Figure 4, session VE7). **C.** Stimulus-induced amplitude modulation at the dominant frequency of the supragranular CSD signal during session V71 (Wilcoxon Signed-Rank test, $p < 0.01$). **D.** Stimulus-induced phase modulation at the dominant frequency of supragranular IT during session V71. As in Figure 1E, post-stimulus phase at the dominant frequency of the ERP was non-random, stimulus presentation induced phase concentration, and the dominant frequency of the pre-stimulus activity differs from the dominant frequency of the ERP. **E.** Median pre- and post-stimulus power spectra for the supragranular tissue of session V71 illustrates stimulus-induced increases in power across frequency bands.

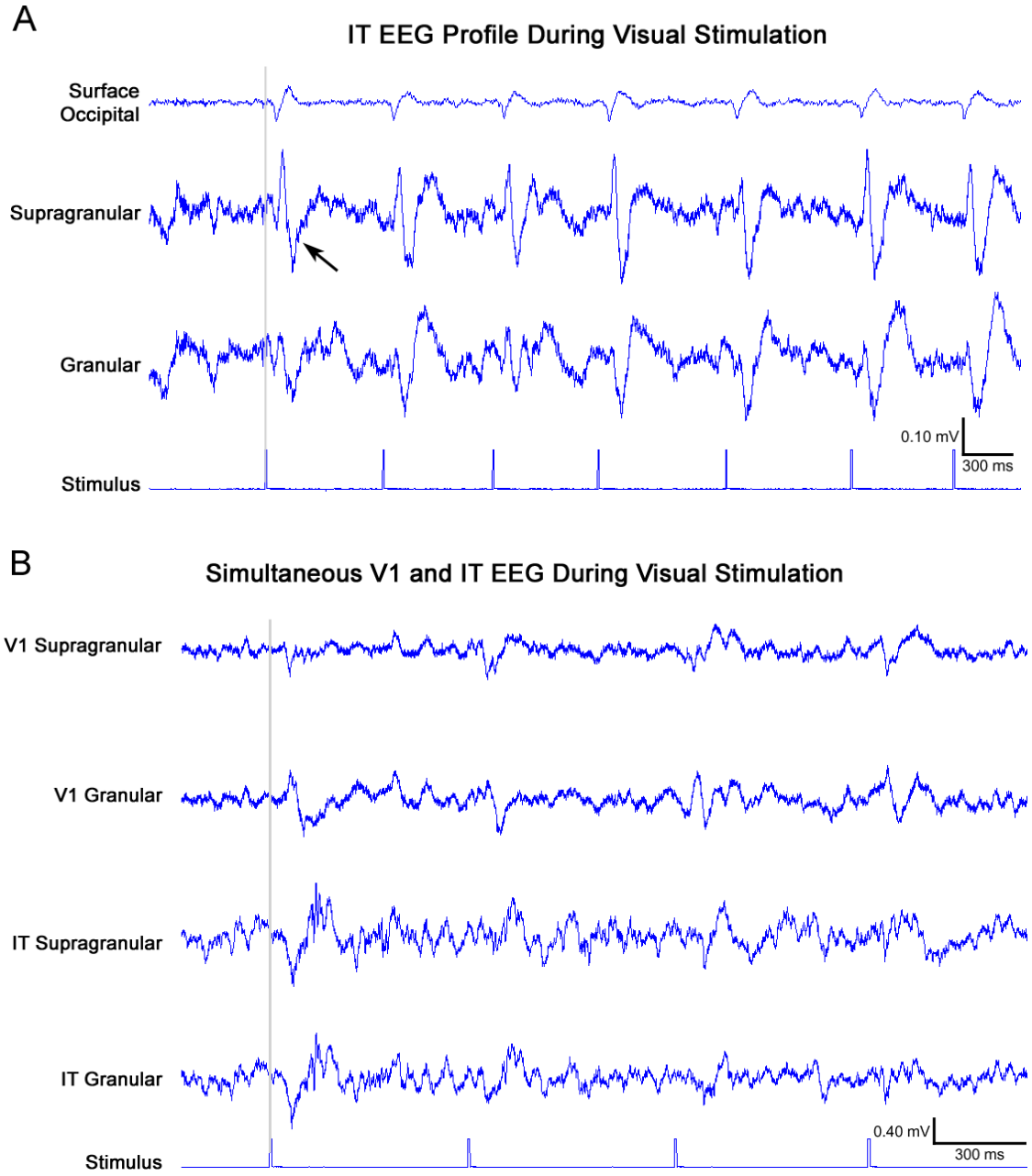
A
IT EEG Profile During Visual Stimulation
Surface Occipital
Supragranular
Granular
Stimulus
0.10 mV
300 ms
B
Simultaneous V1 and IT EEG During Visual Stimulation
V1 Supragranular
V1 Granular
IT Supragranular
IT Granular
Stimulus
0.40 mV
300 ms

Figure 3A-B

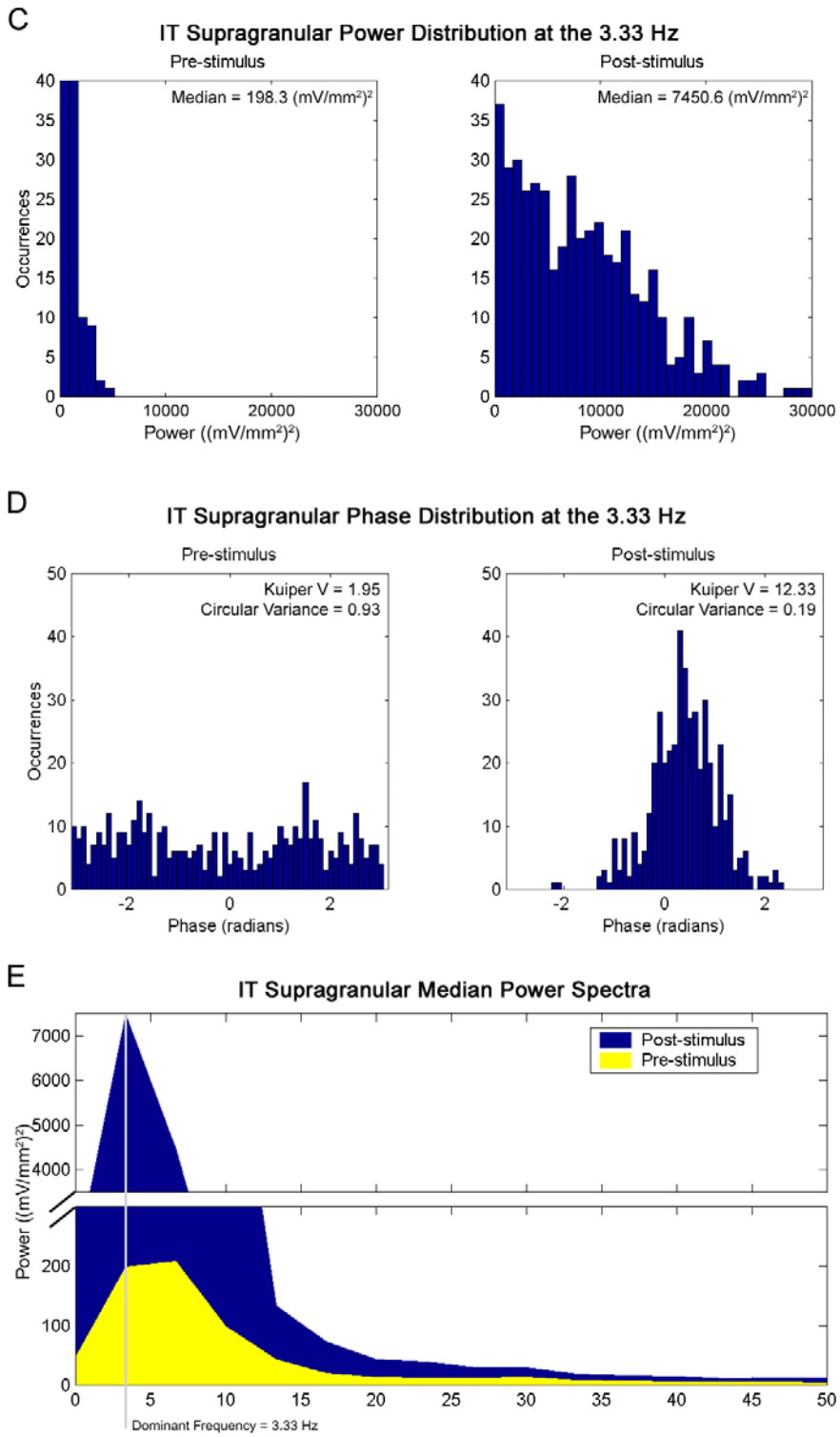
C
IT Supragranular Power Distribution at the 3.33 Hz
Pre-stimulus
Median = 198.3 (mV/mm²)²
Post-stimulus
Median = 7450.6 (mV/mm²)²
Occurrences
Power ((mV/mm²)²)
D
IT Supragranular Phase Distribution at the 3.33 Hz
Pre-stimulus
Kuiper V = 1.95
Circular Variance = 0.93
Post-stimulus
Kuiper V = 12.33
Circular Variance = 0.19
Occurrences
Phase (radians)
E
IT Supragranular Median Power Spectra
Post-stimulus
Pre-stimulus
Power ((mV/mm²)²)
Dominant Frequency = 3.33 Hz

Figure 3C-E

Figure 4: Distribution of normalized total pre- and post-stimulus power in the granular (**A**) and supragranular (**B**) layers of each IT session. See Figure 2 for details.

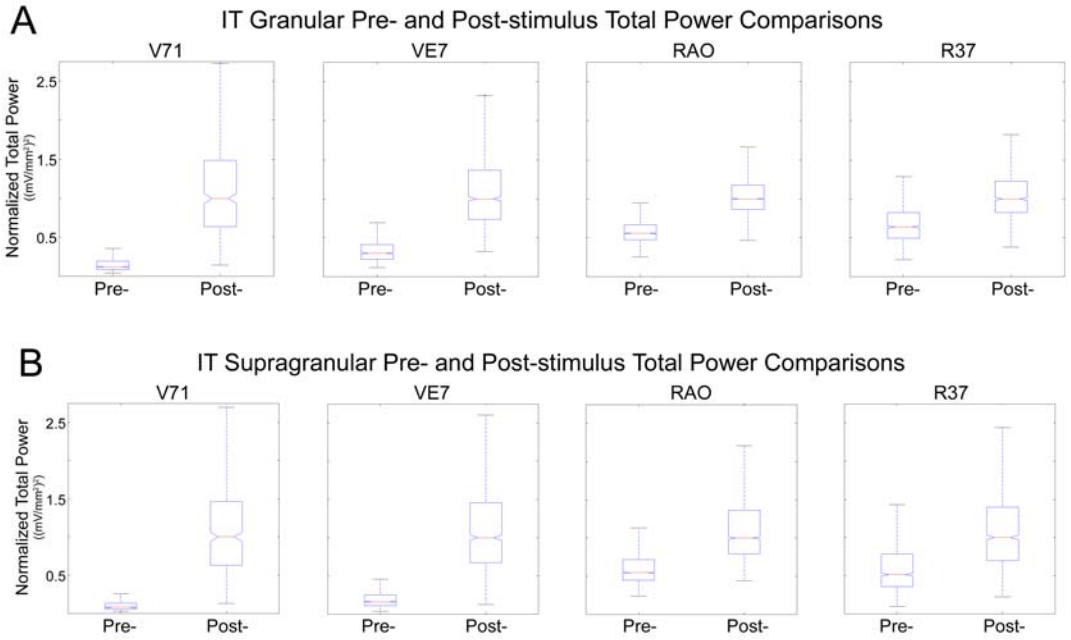

Figure 4

SUPPLEMENTAL MATERIAL

Supplemental Table 1: Dominant frequency (in Hz) of the granular and supragranular current source density signals that were chosen for analysis in each experimental session.

Area	Session	Dominant Frequency	
		Supragranular (Hz)	Granular (Hz)
V1	VA2	3.33 Hz	6.67 Hz
	V66	6.67	3.33
	R47	3.33	6.67
	R69	6.67	6.67
IT	V71	3.33	3.33
	VE7	3.33	3.33
	RAO	6.67	13.33
	R37	3.33	10.00

REFERENCES AND NOTES

1. H. G. Vaughan, Jr., C. E. Schroeder, J. C. Arezzo, in *Slow Activity Changes in the Brain* W. Haschke, E. J. Speckman, Eds. (Birkhauser, Boston, MA, 1992) pp. 111-127.

2. C. E. Schroeder *et al.*, *Electroenceph Clin Neurophysiol* **44**, 55-75 (1995).

3. S. A. Hillyard, T. F. Munte, H. J. Neville, in *Mechanisms of Attention: Attention and Performance XI* M. I. Posner, O. S. Marin, Eds. (Erlbaum, Hillsdale, N.J, 1985) pp. 63-84.

4. S. A. Hillyard, T. W. Picton, in *Handbook of Physiology, Section 1: The Nervous System* F. Plum, Ed. (Oxford University Press, 1987), vol. 5, pp. 519-584.

5. B. M. Sayers, H. A. Beagley, W. R. Henshall, *Nature* **247**, 481-3. (1974).

6. S. Makeig *et al.*, *Science* **295**, 690-4. (2002).

7. First, the data from the high-α condition (Figure 2 of Makeig *et al.* (2002) (*6*)) do not meet important predictions of a Phase Resetting Model. For example, "Resetting" predicts a systematic perturbation of the phase of the ongoing rhythm related to stimulus onset, but no such effect is apparent. Rather, the sorted, single trials suggest that the ongoing rhythms continue unperturbed after stimulus presentation. Second, the authors state that presentation of a stimulus during the negative phase of pre-stimulus alpha activity results in an enhancement of the post-stimulus response in the alpha band. However, Figure 2 (top panel) does not show this; instead, it shows that pre-stimulus phase rotates smoothly through 180 degrees with respect to stimulus onset without there being any point at which amplitude is obviously enhanced or diminished. There is independent support for pre-response activity influencing the event-related potential (*8-10*), however both the Evoked Model and the Phase Resetting Model can incorporate this characteristic. Third, the analysis featured in Figure 2 uses only 20% of the actual data. In order for the authors' argument to have general currency, it is critical that the relationship between N1 and EEG rhythms be detailed over the "middle-α" condition. Finally, ERPs generally consist of a complex mix of frequencies. Narrow band filtering around a dominant frequency (as in Figure 2 (*6*)) would remove evoked responses occurring outside of the band pass of the analysis, and thus, cannot by itself argue against an evoked response contribution to the ERP.

8. M. E. Brandt, B. H. Jansen, J. P. Carbonari, *Electroencephalogr Clin Neurophysiol* **80**, 16-20. (1991).

9. P. Fries, J. H. Reynolds, A. E. Rorie, R. Desimone, *Science* **291**, 1560-3. (2001).

10. P. Fries, S. Neuenschwander, A. K. Engel, R. Goebel, W. Singer, *Nat Neurosci* **4**, 194-200. (2001).

11. For example, Mangun (1992) (*12*) is cited by Makeig *et al.* (2002) (*6*) as supporting the concept of stimulus-induced alterations in neural synchrony (eg. ongoing rhythms). However, Mangun (1992) (*12*) argues that the P1-N1-P2-N2 components recorded at the scalp not lobes of a single oscillatory rhythm but instead each represent manifestations of distinct neural generators.

12. G. R. Mangun, in *Induced Rhythms in the Brain,* E. Basar, Bullock, T.H., Ed. (Birkhauser, Boston, 1992) pp. 217-231.

13. Numerous studies in monkeys show that phasic, stimulus-evoked neural responses contribute to surface ERP components (*2, 12, 14 - 18*).

14. S. J. Givre, C. E. Schroeder, J. C. Arezzo, *Vision Research* **34**, 415-438 (1994).

15. A. D. Mehta, I. Ulbert, C. E. Schroeder, *Cereb Cortex* **10**, 359-70. (2000).

16. C. E. Schroeder, A. D. Mehta, S. J. Givre, *Cerebral Cortex* **8**, 575-592 (1998).

17. C. E. Schroeder, C. E. Tenke, S. J. Givre, *Electroencephalography and Clinical Neurophysiology* **84**, 219-231 (1992).

18. C. E. Schroeder, C. E. Tenke, S. J. Givre, J. C. Arezzo, H. G. J. Vaughan, **31**, 1143-1157 (1991).

19. The dominant frequency of the ERP is the frequency bin of the Fourier-transformed-ERP with the greatest power.

20. J. H. R. Maunsell, W. T. Newsone, *Annual Review of Neuroscience* **10**, 363-401 (1987).

21. A. D. Mehta, I. Ulbert, C. E. Schroeder, *Cerebral Cortex* **10**, 343-358 (2000).

22. For the selective attention experiment, the subjects were presented with random streams of visual and auditory stimuli and were cued to attend to either the visual or the auditory modality at the beginning of each trial block. In each modality, two types of stimuli were presented: a "standard" which was presented during 86% of the trials and a "deviant" which was presented in 14% of the trials. The standard visual stimulus was a red-light flash presented on a diffusing screen subtending 12 retinal degrees and centered on the fixation point. The deviant stimulus differed in intensity or color. The standard and deviant auditory stimuli were pure tone bursts differing in frequency. Eye position was monitored with an infrared eye tracker, and stimuli were presented only when fixation was within a small window around the fixation point. See Mehta *et al.* (2000) (*21*) for further details.

23. Each electrode contact had impedance between 0.l and 0.3 MΩ. Neuroelectric signals were amplified with a pass band of 3-3000 Hz, stored, and subsequently analyzed using a PC-based data acquisition system (Neuroscan, El Paso, Texas).

24. See Schroeder *et al*. (1998) (*16*) for a detailed description of these methods.

25. J. A. Freeman, C. Nicholson, *Journal of Neurophysiology* **38**, 369-382 (1975).

26. Data from each session were prepared for analyses by first epoching EEG data from –300 to 300 milliseconds, with zero denoting stimulus presentation. Second, the average CSD profile was computed, and the laminar positioning of each CSD channel was defined as either supragranular, granular, or infragranular according to the typical (averaged) CSD profile of that cortical area (*16*). Third, the full-wave rectified average CSD signal for each supragranular and granular channel was integrated, and the two channels (one in each sub-layer) with the largest integral areas were chosen for analysis. Fourth, the post-stimulus average CSD (defined as the average CSD waveform from 0 to 300 ms) in these two channels was multiplied by a Hamming window, and the Discrete Fourier Transform (DFT) of the resultant was calculated. The dominant frequency of a layer was then defined as the frequency bin with the greatest power in the spectrum of data from that layer. Fifth, single-trial CSD signals in both chosen channels were split into pre- and post-stimulus signals, multiplied by a Hamming window, and converted to the frequency domain by a 600-point DFT yielding pre- and post-stimulus, single-trial frequency spectra. With a sampling frequency of 2000 Hz and a 600-sample DFT, the frequency bins were 3.33 Hz in width and encompassed 0 to 1000 Hz. Sixth, single-trial power and phase distributions at the dominant frequency (i.e. the frequency bin chosen in step 4 above) were taken from these single-trial spectra.

27. This point is stated and illustrated clearly in Figure 2 of Makeig *et al.* (2002) (*6*) and is critical to the Phase Resetting Model. It should not be confused with the idea that there may be "micro-rhythms" generated by local neuronal ensembles that are de-synchronous and thus immeasurable as an EEG rhythm. If these "micro-rhythms" are present and if they are re-set by the stimulus so that they become organized into a rhythm, then the predictions of this scenario would be indistinguishable from those of the Evoked Model.

28. For simplicity, only 2 recording sites (one granular and one supragranular) are featured in these analyses.

29. N. I. Fisher, *Statistical analysis of circular data* (Cambridge University Press, Cambridge, 1996).

30. Sample circular variance was calculated for the phase data because these values represent a circular population. See Fisher (1996) (*29*) pp. 30-35 for the formulas utilized in this calculation.

31. See Schroeder *et al.* (1998) (*16*) figures 6, 7, 9, 10, 11.

32. Although the N1 is often observed to undergo polarity inversion across the laminar depth of an N1 generator structure, it may not in some instances because volume conduction can superimpose on local activity during the time frame of the N1. In these instances, CSD analysis, which applies a second derivative approximation to the laminar voltage gradient to calculate the underlying source and sink profile (*33*), can be useful to illustrate an active local synaptic response.

33. C. Nicholson, IEEE Trans. Biomed. Engin, BME-20 278-288 (1973).

34. We generally observe large N1s with a lateral-occipital focus, which generally peak around 150 ms, much earlier than the 200 ms shown in Figure 2 of Makeig *et al.* (2002) (*6*). This time course is independent of whether the stimulus is presented foveally or more peripherally, whether it is modulated or unmodulated by an instructional set, or whether it is accompanied with or without α-ringing (*35, 36*).

35. M. M. Murray, J. J. Foxe, B. A. Higgins, D. C. Javitt, C. E. Schroeder, *Neuropsychologia* **39**, 828-44 (2001).

36. G. M. Doniger *et al.*, *J Cogn Neurosci* **12**, 615-21. (2000).

37. R. Bogacz, N. Yeung, C.B. Holroyd (Society for Neuroscience, Online, 2002).

38. G. Rols, C. Tallon-Baudry, P. Girard, O. Bertrand, J. Bullier, *Vis Neurosci* **18**, 527-40. (2001).

39. W. D. Penny, S. J. Kiebel, J. M. Kilner, M. D. Rugg, *Trends Neurosci* **25**, 387-9. (2002).

40. S. A. Hillyard, *Trends in Neurosciences* **8**, 400-405 (1985).

41. M. R. Harter, C. Aine, C. E. Schroeder, *Neuropsychologia* **20**, 421-438 (1982).

ACKNOWLEGDEMENTS

Supported in part by MH060358, T32M07288, IBN0090717, and MH64204. We thank Tammy McGinnis, Noelle O'Connell, and Robert Lindsley for technical support. We also thank Drs. Olivier Bertrand, Steve Hillyard, George Karmos, and Peter Lakatos for numerous discussions and suggestions during the preparation of this manuscript.